An experimental and TD–DFT theoretical study on the photophysical properties of Methylene Violet Bernthsen

ARTICLE *in* DYES AND PIGMENTS · JANUARY 2015

Impact Factor: 3.97 · DOI: 10.1016/j.dyepig.2014.07.022

10 AUTHORS, INCLUDING:

Juan Torres

Universidad Nacional de Río Cuarto

4 PUBLICATIONS **9** CITATIONS

SEE PROFILE

Mariano Vera

Universidad Nacional de Mar del Plata

27 PUBLICATIONS **288** CITATIONS

SEE PROFILE

Carlos A Chesta

Universidad Nacional de Río Cuarto

54 PUBLICATIONS **394** CITATIONS

SEE PROFILE

Hernán A Montejano

Universidad Nacional de Río Cuarto

35 PUBLICATIONS **335** CITATIONS

SEE PROFILE

Dyes and Pigments 112 (2015) 341–351

Contents lists available at ScienceDirect

Dyes and Pigments

journal homepage: www.elsevier.com/locate/dyepig

An experimental and TD-DFT theoretical study on the photophysical properties of Methylene Violet *Bernthsen*

Gabriel E. Jara [a, c], Claudia A. Solis [b], Natalia S. Gsponer [b], Juan J. Torres [b], Carlos A. Glusko [b], Carlos M. Previtali [b], Adriana B. Pierini [c], D. Mariano A. Vera [d, *], Carlos A. Chesta [b, *], Hernán A. Montejano [b, *]

[a] *INQUIMAE-CONICET, Departamento de Química Inorgánica, Analítica y Química Física, Facultad de Ciencias Exactas y Naturales, Universidad de Buenos Aires, Ciudad Universitaria, Buenos Aires, Argentina*
[b] *Departamento de Química, Facultad de Ciencias Exactas, Fisicoquímicas y Naturales, Universidad Nacional de Rio Cuarto, 5800 Río Cuarto, Argentina*
[c] *INFIQC, Departamento de Química Orgánica, Facultad de Ciencias Químicas, Universidad Nacional de Córdoba, Edificio de Ciencias II, Ciudad Universitaria, X5000HUA Córdoba, Argentina*
[d] *Departamento de Química, Facultad de Ciencias Exactas y Naturales, Universidad Nacional de Mar del Plata, Funes 3350, B7602AYL Mar del Plata, Argentina*

ARTICLE INFO

Article history:
Received 12 May 2014
Accepted 16 July 2014
Available online 1 August 2014

Keywords:
Solvatochromism
Pull–push chromophore
TD-DFT
Transient spectra
Non-radiative decay
Stoke's shifts

ABSTRACT

We revisited the photophysics the Methylene Violet (MV) Bernthsen dye in aprotic solvents to rationalize both its peculiar solvatochromism, which cannot be explained by the standard solvatochromic empirical models, and the large dependence of its excited states decay kinetics upon changes on the polarity of the medium.

To this end, MV singlet and triplet excited states were characterized by stationary and time-resolved absorption and emission techniques. The experimental information was combined with a detailed theoretical study using TD-DFT to characterize not only the emitting states but also all dark states which would play a role in determining the fate and properties of the experimentally populated excited states. It is concluded that owning to both the high permanent dipole and polarizability of MV, singlet and triplet excited states are stabilized by the medium to a very different extent, leading to an unusual solvatochromism and decay kinetics.

1. Introduction

Methylene Violet *Bernthsen* (MV, Scheme 1) is a (neutral) synthetic dye that belong to the family of the phenothiazines. Several biological and technological applications for this dye have been reported. Among these, MV has been investigated as a potential photosensitizer for "*in situ*" inactivation of viruses, bacteria and parasites in blood [1–3]. The viability of the cells was also investigated using MV stain which apparently is able to penetrate only dead cells [4]. On the other hand, MV has been used for the amperometric detection of hydrogen peroxide and nicotinamide adenine dinucleotide (NAD) [5] and as an effective inhibitor of steel corrosion in acid media [6].

Several years ago, Otsuki et al. [7,8] reported a study on the photophysical properties of MV (and two closely related derivatives) in aprotic solvents and dioxane-water mixtures. According to these studies, the photophysics of MV is certainly unusual. For instance, a typical Lippert–Mataga plot constructed from the experimental Stokes shifts ($\Delta\nu$) measured in aprotic of low and medium polarity solvents shows a negative slope. Clearly, this behavior cannot be explained in the framework of the current solvatochromic theories. In analogy with the ICT-TICT model [9], Otsuki and col. proposed that MV may exist in (both) the ground and singlet excited states as two conformers, which can rapidly isomerize by means of the rotation of the amine-aromatic ring bond. The fluorescence of the dye arising from two different excited state species (whose predominance could depend on the solvent polarity) may explain the observed anomalies. Recently, Ronzani et al. [10] revised some aspects of MV's photophysics. However, these studies did not provide additional experimental evidence that could be use to confirm Otsuki's hypothesis.

* Corresponding authors. Tel.: +54 3584676523; fax: +54 3584676233.
E-mail address: cchesta@exa.unrc.edu.ar (C.A. Chesta).

http://dx.doi.org/10.1016/j.dyepig.2014.07.022
0143-7208/

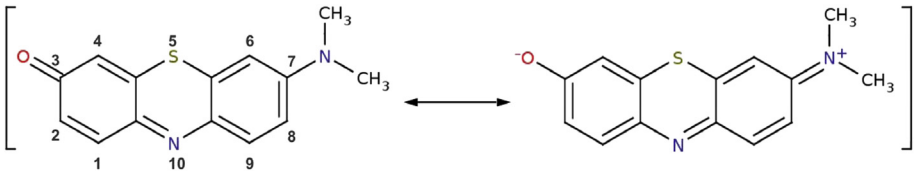

Scheme 1. Methylene Violet (*Bernthsen*) or 3H-phenothiazin-3-one, 7-dimethylamin (MV).

The main aim of this study is to rationalize the sharp dependence of MV photophysics on the nature of the media and to explain its apparent solvatochromic anomalies. Thus, MV singlet and triplet excited states were experimental and theoretically characterized in a series of aprotic solvents covering a broad range of polarities. A simple analysis of the molecular structure of MV shows that it has an electron donor (amino) group coupled to an electron acceptor (carbonyl) group through a conjugated π system. This structure is typical of push–pull chromophores. Although push–pull chromophore have attracted the attention of many researchers because their interesting nonlinear optical properties [11], only few experimental and theoretical studies aimed to achieve a better understanding of the photophysics of this kind of compounds have been reported [12,13].

2. Experimental

2.1. Materials

Methylene violet (Bernthsen) was purchased from Aldrich. The dye content of commercial sample is ~80%, the $-NH_2$ and $-NH(CH_3)$ derivatives being the major impurities [14]. Purification of dye was achieved by flash chromatography on silica (230–400 mesh) using methanol/chloroform 10% v/v as eluent. The purity obtained was >99.9% according HPLC analysis.

All the solvents employed were HPLC grade. The absence of spurious solvent emission was used as purity criterion.

2.2. Methods

UV/Vis absorption spectra were obtained using a Shimadzu UV-2401 spectrophotometer. Steady-state fluorescence measurements were performed on a Fluoromax Spex spectrofluorometer. Freshly prepared MV solutions were used for each measurement and the concentration of the dye adjusted to an absorbance <0.1 to avoid distortion of the spectra due to reabsorption of the emission light. No changes in the absorption or emission spectra and fluorescence lifetimes were observed in the concentration range of 1×10^{-7}–3×10^{-5} M, confirming that the dye does not aggregate at the concentrations used.

Fluorescence quantum yields were determined by integration of the (corrected) emission spectrum using cresyl violet in methanol as fluorescence standard. The reported emission quantum yield of cresyl violet in methanol is 0.54 ± 0.03 [15].

Fluorescence-lifetime measurements were performed with an Edinburgh Instruments OB 900 time-correlated single-photon counting fluorometer. The excitation of the samples was carried-out with a PicoQuant PLS600 diode with emission centered at ~600 nm. The emission wavelengths were selected near maximums of fluorescence bands in each particular solvent. In all cases, the fluorescence lifetimes could be fitted to monoexponential decays, optimizing χ^2, residuals and standard deviation parameters. The lifetimes were independent of the emission and excitation wavelengths.

Transient absorption measurements were carried-out using a laser-flash photolysis equipment. A Spectron SL400 Nd:YAG laser generating 532 nm laser pulses (~18 ns pulse width) was used for sample excitation. The laser beam was defocused in order to cover all the path length (10 mm) of the analyzing beam from a 150 W Xe lamp. The detection system comprises a PTI monochromator coupled to a Hamamatsu R666 PM tube. The signals were captured by an HP54504 digitizing oscilloscope, averaged and finally transferred to a computer for storage and analysis. Measurements were performed in samples deoxygenated by continuous argon bubbling at (25 ± 0.5) °C.

Values of relative permittivities (ε_r), refraction index (n_D), and empirical parameter $E_T(30)$ of pure solvents were obtained from literature [16–18].

2.3. Quantum mechanics calculations

For the Quantum Mechanics calculations, a series of functionals and methodologies were tried for modeling the effect of the solvent. Most calculations were done using the hybrid gradient generalized functionals PBE0 [19], B3LYP [20,21] and its correction proposed by Yanai et al. for accounting the true asymptotic behavior at long interelectronic distances, the CAM-B3LYP [22]. The vertical excitations were computed using the TD-DFT implementation of Gaussian 09 [23]. The state-specific (SS) and linear response (LR) version of the IEFPCM continuum solvation model [24–27] as implemented in Gaussian 09 were applied for modeling heptane, benzene, acetyl acetate and acetonitrile. In all cases the combination of the LR-IEFPCM at the B3LYP/6-311 + G(d,p) level yielded the closer results compared with the experiments and details concerning the other functionals are available as Electronic Supporting Information (ESI). Electrostatic potential and its derived charges as well as the permanent and transition dipole moments computed with CAM-B3LYP and the usual uncorrected form of the functional were practically indistinguishable even though we [28] and other authors [29,30] have observed discrepancies in the charge distribution for systems with much important charge separation and bigger delocalized systems.

The conformational search and optimization of the minima on both the surface of the ground singlet, first triplet and singlet excited states were done the standard procedure by characterizing the stationary points using the diagonalization of the Hessian matrix and harmonic frequencies analysis. The linear response implementation of the IEFPCM was used for all excited states geometry optimizations. The permanent dipoles, electrostatic potentials, total electron density and spin distribution of the electronic states were done and plotted using the LR generalized CI density matrix using Molden [31] and VMD 1.8.9 [32] graphical packages.

3. Results and discussion

3.1. Ground and singlet excited states properties

The absorption and (corrected) emission spectra of the MV were acquired in a series of aprotic solvents covering a wide range of solvent polarities (Table 1). The absorption and emission spectra of

Table 1
Absorption and fluorescence maxima, absorption coefficients, emission lifetimes, and fluorescence quantum yields of MV in protic solvents.

Solvent	E_T^N	ν_A^{max}/ cm^{-1}	ν_F^{max}/ cm^{-1}	ε/M^{-1} cm^{-1} (f)	τ_F/ns	Φ_F
c-hexane	0.006	19,417	15,963	30,000 (0.44)	0.25	0.002
n-heptane	0.009	19,512	16,000	–	0.29	0.002
dibutyl ether	0.071	19,201	15,637	31,500 (0.47)	0.28	0.013
benzene	0.111	18,769	15,361	–	0.88	0.088
ethyl acetate	0.228	18,650	16,380	32,000 (0.48)	1.30	0.107
dichlorometane	0.309	18,228	16,207	–	1.54	0.153
1,2-dichloroethane	0.327	18,202	16,181	–	1.68	0.199
acetone	0.355	18,215	16,051	–	1.81	0.198
butanitrile	0.364	18,255	16,103	–	1.93	0.203
propionitrile	0.398	18,175	16,038	–	1.70	0.167
acetonitrile	0.460	18,136	16,026	33,000 (0.50)	1.60	0.194

MV recorded in *c*-hexane, butyl ether, ethyl acetate and acetonitrile are shown in Fig. 1.

The absorption band undergoes an apparent shift to lower energies with increasing solvent polarity. This shift is accompanied by slight changes in the spectral shapes. The observed solvatochromic effect suggests a large ground-state dipole moment (μ_G). The molar absorption coefficients (ε) and the corresponding oscillator strengths (f) measured in a series of aprotic solvents are reported in Table 1 and Table 2a. The emission spectrum also shifts to lower energies with increasing solvent polarity. However, in contrast to that observed for the absorption, the emission spectra show well-defined vibrational progressions in all solvents studied. It is also apparent the complete lack of a "mirror" symmetry between the absorption and emission spectra. This is a typical behavior of push–pull chromophores. The estimation of the transition energies when major changes in the relative vibronic intensities are observed has been rarely discussed in the literature. In the practice, different strategies have been adopted. Some authors have chosen to report the transition's average energies [33] or the 0–0 absorption and emission energies estimated by fitting the corresponding spectra to single-mode Franck–Condon expressions [34]. However, other researchers have strongly suggested that the energy of the (absorption/emission) absolute maxima should be always reported and analyzed [12]. We report herein the energy of the absorption (ν_A) and emission (ν_F) absolute maxima. The corresponding values are collected in Table 1.

Solvent effects on the Stock's shifts ($\Delta\nu$) are usually analyzed using expressions like:

$$\Delta\nu = \frac{\Delta\mu^2}{a^3}S + C \tag{1}$$

where: $\Delta\mu(=\mu_E - \mu_G)$ represents the difference between the dipole moments of the first singlet excited and ground states, respectively, a is the radius of the Onsager's solvent cavity and S a theoretical (or empirical) solvent parameter. In this article, Ravi's solvatochromic model [35] was used because it successfully accounts for both specific and non-specific fluorophore/solvent interactions. Ravi's solvatochromic parameter (S_R) reads:

$$S_R = \frac{11307.6a_B^3}{\Delta\mu_B^2}E_T^N \tag{2}$$

where E_T^N is the normalized empirical microscopic solvent polarity parameter [36]. In Equation (2), a_B(6.2 Å) and $\Delta\mu_B$(9.0 D) represent the solvent cavity radius and the dipole moment change measured for the reference dye pyridinium *N*-phenolate betaine B [15], respectively. Since: $\Delta\mu^2 \geq 0$, Equation (1) predicts that a

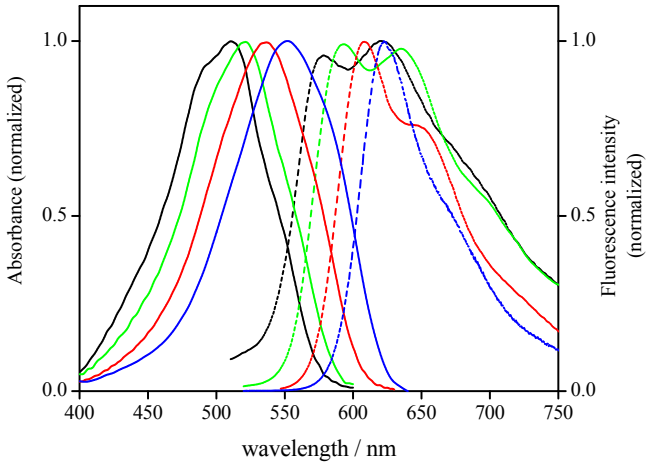

Fig. 1. Normalized absorption (left) and fluorescence (right) spectra measured of MV (~3 × 10^{-6} M) in *c*-hexane (black), butyl ether (green), ethyl acetate (red) and acetonitrile (blue). All experiments were carried-out at 298 K. (For interpretation of the references to colour in this figure legend, the reader is referred to the web version of this article.)

representation of $\Delta\nu$ *vs.* E_T^N should be linear and show positive slope. Several examples of this behavior have been reported [35,37]. However, it is important to note that most solvatochromic models (including Ravi's one) involve a large number of approximations. For instance, it is being assumed that the dipole moments of the vertical FC singlet excited state S_1 (μ_E) and the fully (geometry and solvent) relaxed state S_1^* (μ_E^*) singlet excited states are the same. Similarly, the dipole moments of the relaxed S_0 (μ_G) and unrelaxed FC S_0^* (μ_G^*) ground states are considered as identical. These assumptions are not always satisfied, particularly when easily polarizable chromophores (such as push–pull chromophores) are being studied. In such cases, it is convenient to analyze the solvent effects on ν_A, ν_F and$\Delta\nu$ according Equations (3)–(5): [38,39]

$$\nu_A = \frac{\mu_G(\mu_G - \mu_E)}{a^3}S_R + C_A \tag{3}$$

$$\nu_F = \frac{\mu_E^*(\mu_G^* - \mu_E^*)}{a^3}S_R + C_F \tag{4}$$

$$\Delta\nu = \nu_A - \nu_F = \frac{\mu_G(\mu_G - \mu_E) - \mu_E^*(\mu_G^* - \mu_E^*)}{a^3}S_R + C \tag{5}$$

where C_A, C_F and C are characteristic constants for the chromophore studied. The values of ν_A, ν_F and the corresponding $\Delta\nu$ measured for MV in the different solvents are plotted as a function of E_T^N in Fig. 2. As shown, the absorption and emission wavenumbers decrease with increasing E_T^N. However, the dependence is not linear as predicted by Equations (3) and (4). Similar correlations are obtained when the experimental data are plotted against the Lippert–Mataga [40] or Bakhshiev's [41] solvatochromic parameters. Interestingly, the $\Delta\nu$ also decrease with increasing E_T^N in sharp contrast with the behavior predicted by Equation (1), and in agreement with the results previously reported by Otsuki et al. [7,8]

The solvent effects on the fluorescence quantum yields (Φ_F) and the emission lifetimes (τ_F) were also investigated. The experimental values of Φ_F and τ_F are listed in Table 1. As noted by Otsuki et al. [7], both photophysical parameters markedly depend on the polarity of the medium. In alkane solvents, MV is barely fluorescent. However, Φ_F quickly increases with increasing media polarity reaching a plateau value of ~0.2 in the more polar solvent series. The emission

Table 2a
Theoretically predicted singlet excited state energies (ΔE/cm^{-1}), oscillator strengths (f) and dipole moments (μ) calculated for some relevant states of MV in vacuum, *c*-hexane, *n*-heptane, butyl ether, ethyl acetate, dichloromethane, acetone and acetonitrile. Data corresponding to the only (or most intense) absorption band is in bold.

Solvent	E_T^N		ΔE/cm^{-1}	Transition	Transition type	f	μ/D	$\Delta\lvert\mu\rvert$/D	θ/deg
Vacuum	0.000	S_0	0	–	–	–	10.7		
		S_1	21,142	$H_{-2} \rightarrow L$	$n \rightarrow \pi^*$	0.000	5.5	−5.3	12.2
		S_2	**21,530**	$H \rightarrow L$	$\pi \rightarrow \pi^*$	0.466	12.0	1.3	5.18
		S_3	23,465	$H_{-1} \rightarrow L$	$\pi \rightarrow \pi^*$	0.137	14.8	4.1	5.48
c-Hexane	0.006	S_0	0	–	–	–	13.3		
		S_1	**20,297**	$H \rightarrow L$	$\pi \rightarrow \pi^*$	0.756	15.6	2.3	2.7
		S_2	21,924	$H_{-2} \rightarrow L$	$n \rightarrow \pi^*$	0.000	6.5	−9.1	12.8
		S_3	22,544	$H_{-1} \rightarrow L$	$\pi \rightarrow \pi^*$	0.061	16.6	1.0	7.2
Heptane	0.009	S_0	0	–	–	–	12.9		
		S_1	**20,390**	$H \rightarrow L$	$\pi \rightarrow \pi^*$	0.737	15.4	2.5	2.8
		S_2	21,872	$H_{-2} \rightarrow L$	$n \rightarrow \pi^*$	0.000	6.4	−6.5	12.8
		S_3	22,600	$H_{-1} \rightarrow L$	$\pi \rightarrow \pi^*$	0.064	16.5	3.6	7.1
Dibutyl ether	0.071	S_0	0	–	–	–	14.0		
		S_1	**19,652**	$H \rightarrow L$	$\pi \rightarrow \pi^*$	0.882	17.3	3.3	2.1
		S_2	22,165	$H_{-2} \rightarrow L$	$n \rightarrow \pi^*$	0.000	8.0	−9.3	12.5
		S_3	22,308	$H_{-1} \rightarrow L$	$\pi \rightarrow \pi^*$	0.038	18.9	4.8	4.3
Ethyl acetate	0.228	S_0	0	–	–	–	15.8		
		S_1	**18,854**	$H \rightarrow L$	$\pi \rightarrow \pi^*$	1.020	19.3	3.5	1.6
		S_2	21,738	$H_{-1} \rightarrow L$	$\pi \rightarrow \pi^*$	0.021	18.8	2.9	8.1
		S_3	22,782	$H_{-2} \rightarrow L$	$n \rightarrow \pi^*$	0.000	7.5	−8.4	13.9
DCM	0.309	S_0	0	–	–		16.5		
		S_1	**18,535**	$H \rightarrow L$	$\pi \rightarrow \pi^*$	1.072	20.1	4.3	1.5
		S_2	21,576	$H_{-1} \rightarrow L$	$\pi \rightarrow \pi^*$	0.017	19.3	2.8	8.2
		S_3	22,988	$H_{-2} \rightarrow L$	$n \rightarrow \pi^*$	0.000	7.7	−8.8	14.3
Acetone	0.355	S_0	0	–	–		16.7		
		S_1	**18,120**	$H \rightarrow L$	$\pi \rightarrow \pi^*$	1.137	21.1	5.2	1.4
		S_2	21,365	$H_{-1} \rightarrow L$	$\pi \rightarrow \pi^*$	0.014	20.0	3.3	4.1
		S_3	23,235	$H_{-2} \rightarrow L$	$n \rightarrow \pi^*$	0.000	7.9	−8.7	10.5
Acetonitrile	0.460	S_0	0	–	–		17.7		
		S_1	**17,977**	$H \rightarrow L$	$\pi \rightarrow \pi^*$	1.159	21.4	3.7	1.3
		S_2	21,293	$H_{-1} \rightarrow L$	$\pi \rightarrow \pi^*$	0.013	20.2	2.6	8.4
		S_3	23,330	$H_{-2} \rightarrow L$	$n \rightarrow \pi^*$	0.000	8.0	−9.7	14.9

lifetime show a similar trend; τ_F increases from ~0.3 ns in the less polar solvents to >1.6 ns in polar media.

Fig. 3(a) shows a plot of the experimental absorption energies ν_A *vs*. the corresponding (vertical) excitation values calculated using the TD-DFT approach. The ideal correlation, *i.e.*: $\nu_A(exp) = \nu_A(cal)$, is represented by a dotted line. As shown in Fig. 3(a), the trend of solvent effects on the absorption maxima is well reproduced ($R^2 = 0.982$). However, the experimental ν_A are overestimated. In the less polar solvents, the calculated ν_A deviates from the experimental values by ~600–900 cm^{-1}. It is worth to note that the excitation energies computed at the TD-DFT level of theory are estimated to be accurate within 2000–3000 cm^{-1}, usually requiring a shift towards the red to reproduce experimental absorption spectra [13b,42]. Therefore, the overall correlation can be considered satisfactory, allowing the analysis of calculated molecular properties of the dye to rationalize the solvent effects on its photophysics.

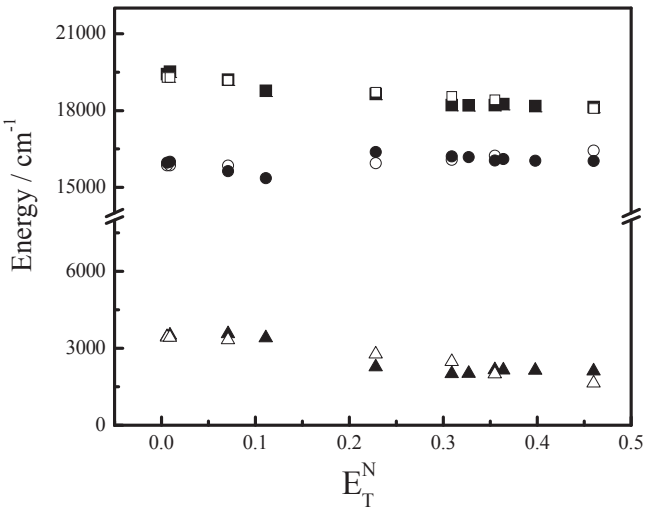

Fig. 2. Experimental ν_A (■), ν_F (●) and Stokes shifts ($\Delta\nu$) (▲) calculated from the absolute spectrum maxima as a function of the solvatochromic parameterE_T^N. Empty symbols represent the theoretically calculated quantities (see the main text for details).

As shown in Table 2a the dipole moment of the ground state (μ) significantly increases with increasing polarity of the medium. The solvent effects on the main (one-electron) orbital energies of the ground MV MO's are shown in the ESI Fig. S1. The main orbitals involved in the $S_0 \rightarrow S_1$ and $S_0 \rightarrow S_2$ transitions are stabilized to a different extent as the polarity of the medium increases. As discussed below, this fact plays a key role in the properties of the resulting all-electron final singlet states in the TD-DFT expansion and explains most solvatochromic effects. However, at this point we first checked the possibility of the existence of two absorbing states, as suggested by Otsuki et al., by studying the conformational profile of the ground MV. As summarized on the ESI Fig. S2, the structure with the Me_2N– group nearly perpendicular to the aromatic rings plane was found to be just the transition state between the two equivalent poses lying on the plane. The lowest barrier was found in the less polar medium, c-hexane, it being 8.9 kcal/mol; in the most polar one, it resulted even higher, 10.7 kcal/mol. Thus, it seems unlikely the existence of two different conformers involved in the absorption at room temperature. A slightly more complex study on the surface of the possible lowest energy singlet excited states will be discussed later in order to evaluate the possibility of two emitting states in fast equilibrium in regards to the fluorescence spectra.

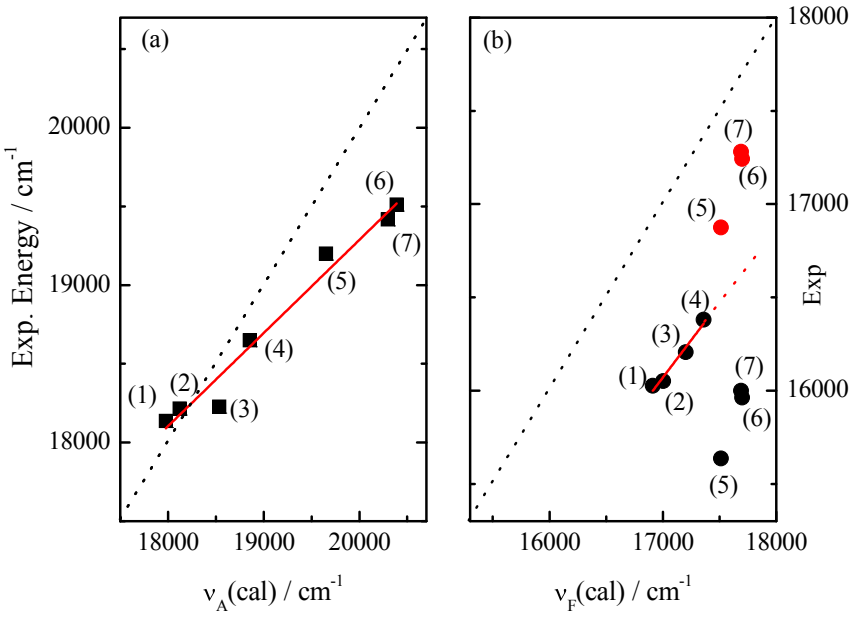

Fig. 3. Experimental $\nu(exp)$*vs.* theoretically calculated $\nu(cal)$ absorption (a) and emission (b) energies in the series of solvent studied. Black and red circles in Fig. 3(b) represent the emission energy measured at the maximum (0–1) and at the first (0–0) vibronic transitions, respectively. The dotted line represents the ideal correlation: $\nu(exp) = \nu(cal)$. Solvents: acetonitrile (1), acetone (2), dichloromethane (3), ethyl acetate (4), butyl ether (5), *n*-heptane (6) and c-hexane (7). (For interpretation of the references to colour in this figure legend, the reader is referred to the web version of this article.)

The vertical excited states $\Delta E(S_0 \rightarrow S_n)$ found by TD-DFT simulations are listed in Table 2a and plotted as a function of E_T^N in Fig. 4.

Although there is no spectrum of MV available in the gas phase, it is worth to note that in vacuum the lowest $n \rightarrow \pi^*$ transition leads the first excited state S_1 (green triangles, Fig. 4). This transition involves a charge transfer in the opposite direction of the dipole moment of S_0 causing a significant decrease in the μ of S_1 (negative $\Delta\mu$, Table 2a). Since the starting *n* orbital is localized on the carbonyl, it is strongly stabilized by polar solvents. In contrast, the final π^* orbital is mostly delocalized and therefore, it is much less sensible to the medium. Hence, the energy gap between the two orbitals progressively increases with increasing solvent polarity shifting the $n \rightarrow \pi^*$ transition to higher energies. Note that this transition becomes S_2 in *n*-heptane and S_3 in the more polar solvents (Fig. 4). As expected by orbital symmetry, this transition has no intensity ($f \sim 0$) and it is not observed in the experimental spectra. In contrast, the lowest $\pi \rightarrow \pi^*$ transition (red circles, Fig. 4), which corresponds to S_2 in the gas phase, becomes S_1 in *n*-heptane and it continues red-shifting with increasing solvent polarity because it always involves a positive $\Delta\mu$ (Table 2a).

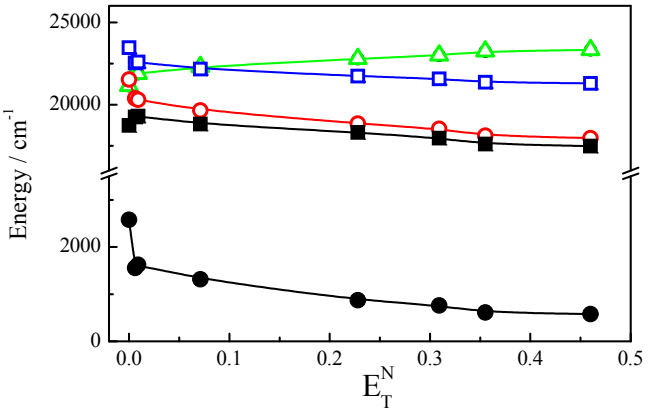

Fig. 4. Calculated energy gaps: $\Delta E(S_0 \rightarrow S_n)$, for $n = 1,2,3$ (empty symbols; red, blue and green color codes correspond to the states which are mainly HOMO → LUMO, HOMO-1 → LUMO and HOMO-2 → LUMO, respectively), $\Delta E(S_0 \rightarrow S_1^*)$ (■) and $\Delta E(S_0 \rightarrow S_0^*)$ (●) as a function of E_T^N (see the main text for details). (For interpretation of the references to colour in this figure legend, the reader is referred to the web version of this article.)

Thus, the sensitivity of the $S_0 \rightarrow S_1$ transition to the polarity can be explained in terms of the greater degree of asymmetry of the electron density of the final state (S_1) compared to that of the initial state (S_0). This fact is clearly depicted in Fig. 5 for the case of ethyl acetate. In this solvent of intermediate polarity, the dipole moment (μ) raises from 15.8 D (S_0) to 19.3 D (S_1) upon excitation.

The increase in electron density on the leftmost ring (Fig. 5) and in particular, on the endocyclic S and N atoms (which are nodal in the π HOMO and maximum in the π^* LUMO), is build-up at expense of a decrease of the electron density of the exocyclic nitrogen (the p_z AO contribution of this N is greater in the HOMO than in the LUMO). Orbitals and transition density isosurface plots are available as ESI (Figs. S1 and S3, respectively). In all cases, the μ of S_1 and S_0 are nearly collinear. As shown in Table 2a, the angle between the μ vectors increases as the polarity of the media decreases, reaching the maximum in the gas phase.

The $S_0 \rightarrow S_1$ transition has a single determinantal character in the resulting CI expansion, being essentially HOMO → LUMO in all solvents studied. However, a small contribution (with coefficients ~0.1) of the HOMO-1 → LUMO Slater's determinant is also apparent in the less polar solvents. The absorption intensities are acceptably reproduced by the simulations (f in Table 2a) within the errors inherent to the TD-DFT methods. The decreased oscillator strength (f) calculated for the less polar solvents (in agreement with the experimental molar absorption coefficients) can be ascribed to the above mentioned contribution of other Slater's determinants to the $S_0 \rightarrow S_1$ transition. The HOMO-1 → LUMO configuration is also $\pi \rightarrow \pi^*$ and in most solvents, responsible for the S_2 excited state ~440–470 nm (blue squares, Fig. 4). However, this transition is inherently weak ($f \sim 0.06$–0.01) and therefore, undetectable due its proximity to the much more intense $S_0 \rightarrow S_1$ band. Hence, the

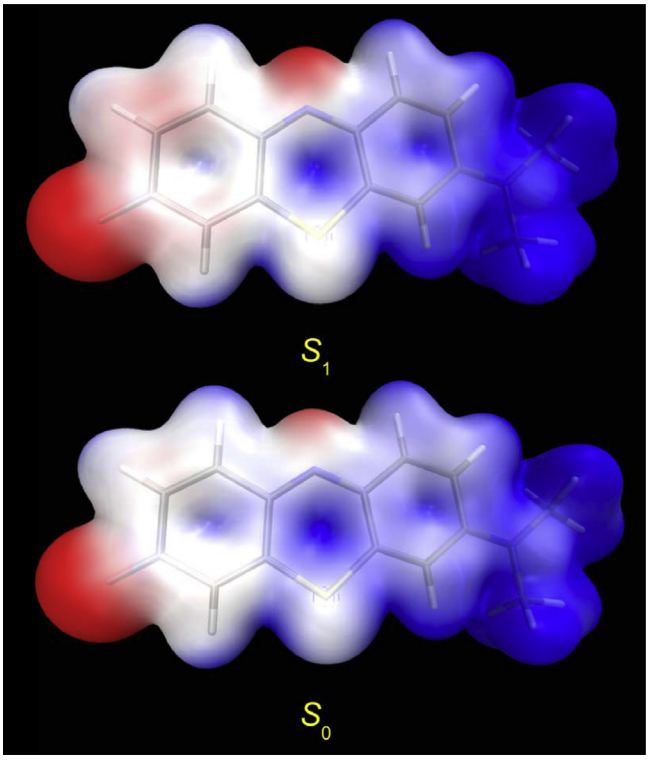

Fig. 5. Electron density isosurfaces of 0.01 a. u. obtained for S_0 and S_1 states colored according to the molecular electrostatic potential; it ranging from −0.1 a.u (red) to +0.1 a.u. (blue). Solvent: ethyl acetate. (For interpretation of the references to colour in this figure legend, the reader is referred to the web version of this article.)

solvent effect on *f* for the $S_0 \rightarrow S_1$ and $S_0 \rightarrow S_2$ transitions can be rationalized in terms of the progressive mixing of both Slater's determinants with decreasing solvent polarity.

The relevant states for the emission are the relaxed singlet S_1^* and the unrelaxed ground state S_0^*. As shown in Fig. 3(b) (and Table 2b), the calculated TD-DFT energies associated to the $S_1^* \rightarrow S_0^*$ transition nicely reproduce the trend of the experimental ν_F for acetonitrile, acetone, dichloromethane and ethyl acetate. The experimental ν_F are overestimated by ~1000 cm^{-1}, error that is still acceptable within the TD-DFT approach. The ν_F calculated for the less polar solvents studied (*c*-hexane, *n*-heptane and *t*-butyl ether) clearly fall outside the correlation. This behavior can be rationalized comparing the fluorescence spectra in Fig. 1. Note that for *c*-hexane (and for *t*-butyl ether when the emission spectrum is represented in wavenumbers), the emission maximum agrees with that of the second (0–1) vibronic state. Splitting of the maxima onto two vibronic peaks of similar intensity has no parallel in the more polar solvents of the series. In the polar solvents, the 0–0 vibronic state has a clearly predominant contribution. Interestingly, when the energy of the 0–0 vibronic state (for *c*-hexane, *n*-heptane, and *t*-butyl ether) is plotted instead the ν_F maxima, the correlation in Fig. 3(b) does not show any significant improvement. At this point, it is important to recall the TD-DFT calculated energy for the $S_1^* \rightarrow S_0^*$ transition does not takes into account the Huang–Rhys factors, which ultimately determine the relative intensities of the vibronics of the emission (and absorption) spectra.

In principle, the change in the vibronic profile in the fluorescence spectra can be ascribed to a larger displacement of the equilibrium geometry of S_1^* (with respect either to that of S_0 or S_1) in the less polar media. A closer analysis of the computed properties of S_1^* and S_0^* seems to support this hypothesis. Relaxation from S_1 to S_1^* leads to the stabilization of the excited state (Fig. 4), but it also involves a decrease of μ and a change in the molecular geometry. A similar behavior is observed when S_0^* and S_0 are compared. Note that the energy required to reach the equilibrium geometry of the unrelaxed ground state from S_0 (Fig. 4 and Table 2b) is relatively low in polar solvents (~500-800 cm^{-1}), whereas it varies from 1320 to 2580 cm^{-1} in going from *t*-butyl ether to vacuum. The MV's equilibrium geometries of S_0^* (or S_1^*) and S_0 (or S_1) in *c*-hexane are compared in Fig. S4-ESI. The changes in the geometry, measured as the root mean square deviation (RMSD) of the internal coordinates, was found to be around 0.07 Å for the alkanes solvents and only about 0.03–0.01 Å for the polar series (from ethyl acetate to

Table 2b
Summary of relevant states calculated for the $S_1^* \rightarrow S_0^*$ emission transition of MV in vacuum, *c*-hexane, *n*-heptane, butyl ether, ethyl acetate, dichloromethane, acetone and acetonitrile. The energy values for S_0^* reported where calculated relative to S_0 for each solvent.

Solvent	E_T^N		$\Delta E/cm^{-1}$	$S_1^* \rightarrow S_0^*/cm^{-1}$	Main transition	Transition type	*f*	μ/D	$\Delta\lvert\mu\rvert$/D	θ/deg
Vacuum	0.000	S_0	0	–	–	–	–	10.7		
		S_0^*	2579					12.4		
		S_1^*	18,747	16,168	$L \rightarrow H_{-2}$	$n \rightarrow \pi^*$	0.000	7.4	5.0	9.1
c-Hexane	0.006	S_0	0					13.3		
		S_0^*	1555					14.4		
		S_1^*	19,251	17,699	$L \rightarrow H$	$\pi \rightarrow \pi^*$	0.432	13.9	0.5	6.2
n-Heptane	0.009	S_0	0					12.9		
		S_0^*	1624					14.2		
		S_1^*	19,314	17,690	$L \rightarrow H$	$\pi \rightarrow \pi^*$	0.406	13.7	0.5	6.4
Dibutyl ether	0.071	S_0	0					14.3		
		S_0^*	1318					15.7		
		S_1^*	18,831	17,513	$L \rightarrow H$	$\pi \rightarrow \pi^*$	0.597	15.5	0.2	4.9
Ethyl acetate	0.228	S_0	0					15.8		
		S_0^*	872					17.2		
		S_1^*	18,231	17,359	$L \rightarrow H$	$\pi \rightarrow \pi^*$	0.848	17.7	−0.5	3.2
DCM	0.309	S_0	0					16.5		
		S_0^*	764					17.8		
		S_1^*	17,968	17,203	$L \rightarrow H$	$\pi \rightarrow \pi^*$	0.946	18.7	−0.9	2.6
Acetone	0.355	S_0	0					16.6		
		S_0^*	611					18.6		
		S_1^*	17,615	17,004	$L \rightarrow H$	$\pi \rightarrow \pi^*$	1.052	19.9	−1.3	2.1
Acetonitrile	0.460	S_0	0					17.7		
		S_0^*	577					18.9		
		S_1^*	17,488	16,911	$L \rightarrow H$	$\pi \rightarrow \pi^*$	1.085	20.4	−1.43	1.97

acetonitrile). Since the Huang-Rhys factor is a quantitative measure of the geometry distortion of S_1^*(relative to the ground state), these results justify the changes in the relative intensities of vibronics in going from polar (0–0) to non-polar solvents (1–0).

The solvent effects on the energies of the most relevant excited states close toS_1^* are shown in Fig. 6. All energies (relative toS_0 in each solvent) were calculated at the geometry of S_1^*.

In all solvents, the relaxed singlet states (S_1^*'s) has mixed contributions of HOMO → LUMO and HOMO-1 → LUMO Slater's determinants. The degree of mixing depends on the polarity of the medium. The S_1^* found in the ethyl acetate to acetonitrile series have large contributions (~0.9) of the HOMO → LUMO transition. In contrast, in *n*-heptane and *c*-hexane, the contributions from HOMO → LUMO and HOMO-1 → LUMO Slater's determinants are in the order of 0.65 and 0.25, respectively. For *t*-butyl ether, these coefficients are ~0.68 and ~0.20. This mixing is consistent with the proximity of S_2^*(~1800 cm^{-1} above in *n*-heptane) for which the main Slater determinant corresponds to the HOMO-1 → LUMO excitation. As in the case of the absorption, the HOMO-1 → LUMO configuration is also π → π* but characterized by a relatively small oscillator strength (*f*). This variable degree of mixing can be use to explain several aspects of MV's photophysics. Note that the *f* calculated for the emission in the alkane's solvents is ~0.4; this is, nearly half the calculated for the absorption process in the same solvents. However, in polar media, the *f* estimated for the emission and absorption transitions are similar. Another peculiarity of the system studied is the solvent effect on the Δμ associated to the $S_1^* \rightarrow S_0^*$ transition. In the polar series (from ethyl acetate to acetonitrile) Δμ is negative, indicating that the unrelaxed ground state S_0^* is less polar than S_1^*(as observed for the absorption process). In contrast, for the less polar solvent series (n-hexane to butyl ether) Δμ is positive, which implies that S_0^* is characterized by a larger dipole moment than S_1^*. As discussed at the end of this section, these changes in *Δμ* are consistent with the observed solvent effects on ν_F.

Even though the above considerations consistently rationalize the observed solvent effects on ν_F, an exploration of the potential energy surface of S_1^* was performed in order to check the hypothesis of two emitting states proponed by Otsuki et al.. The rotation of the Me_2N-group in the surface of the relaxed S_1^* resulted even more

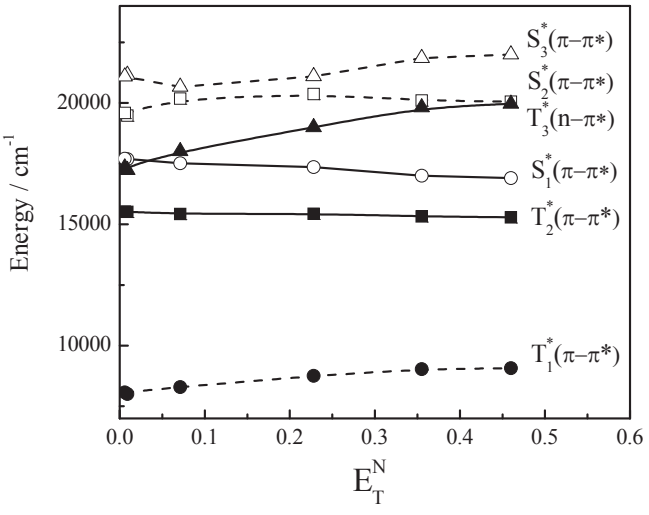

Fig. 6. Energies of the most relevant excited states close to S_1^* upon change on the polarity of the media calculated at the geometry of S_0. All calculated energies are relative to that of S_0 in each solvent. Solvents: *c*-hexane (E_T^N = 0.006), *n*-heptane (0.009), ethyl acetate (0.228), acetone (0.355) and acetonitrile (0.460). Singlet and triplets states are represented by open and solid symbols, respectively.

restrained than in the ground state (13.5 kcal/mol in the case of acetonitrile). Results are summarized on ESI Figs. S5 and S6 for acetonitrile and c-hexane, respectively, as edges of the polarity range. The structure of higher energy with the Me_2N-perpendicular to the rings plane features an sp^3 hybridization on the nitrogen. From this transition state, the system could either relax to the geometry of S_1^* discussed so far or to another structure of similar energy, also with the Me_2N-perpendicular to the phenotiazyne plane but with an sp^2 nitrogen, it displaying a larger charge separation. However, and despite the low probability of such energetic rearrangements on the excited surface, the calculated oscillator strength (*f*) for the emission from this structure *is zero*, thus no experimental trace about this state would be observed. Moreover, either in acetonitrile or *c*-hexane the profiles are similar. Therefore, the existence of two emitting states in fast equilibrium as the source of the changes in the emission with the increasing solvent polarity seems unlikely.

The dependence of ν_A, ν_F and $\Delta\nu$ on the solvent polarity (Fig. 2) can be modeled using the theoretically calculated μ of the four states involved in the absorption/emission processes (Table 2a and 2b). To this end, the experimental values of ν_A and ν_F were (globally) fitted to Equations (3) and (4), leaving a^3, C_A and C_F as adjustable parameters. The fitting retrieved values of 7.8 Å, 19,400 and 16,000 cm^{-1} for *a*, C_A and C_F, respectively. Results are shown in Fig. 2 as empty symbols. As it may be concluded, the fit is acceptable and explain the anomalies originally observed by Otsuki et al.. For most fluorescent probes: $\mu_G \cong \mu_G^*$, $\mu_E \cong \mu_E^*$ and $\mu_E > \mu_G$, being a good approximation to consider all dipole moments as solvent independent. In such case, a plot of ν_A or ν_F, according to Equations (3) and (4), generally shows straight lines with negative slopes. Since $\mu_E > \mu_G$, the slope observed for ν_F is necessarily larger than that observed for ν_A. As a result, the representation of $\Delta\nu$ *vs*. S_R shows a positive slope. However, this is not the case for MV. For this dye (and other pull–push chromophores), the electron donor and electron acceptor moieties (Scheme 1) are strongly coupled, making the dye structure highly (electronically) polarizable. This is, the distribution of electron density of MV (and therefore its μ) easily adjusts to the medium. This becomes apparent by comparing the values of μ_G (Table 2a) and μ_G^* (Table 2b). Note that in all solvents the μ of S_0^* exceeds that of S_0. This is possible because during the $S_1^* \rightarrow S_0^*$ transition, the nuclear polarization of the solvent is maintained so, in order to minimize the free Gibbs energy change of the system, the dye (ground state) dipole moment increases to compensate the polarization of the solvent cage. The main consequence of this is a decreased $(\mu_G^* - \mu_E^*)$ which explains the (abnormally) law slope of the ν_F *vs*. S_R plot (see Fig. 2).

3.2. Triplet excited state properties

Recently, Ronzani et al. [10] published for the first time the triplet–triplet absorption spectrum of MV in acetonitrile. In this article, the studies on the MV's excited triplet state properties are extend to less polar solvents and fully characterized. The transient (difference) absorption spectrum of MV in (deoxygenated) ethyl acetate is given in Fig. 7.

The spectrum shows positive absorptions between 350–450 and 600–850 nm. It is also apparent a negative absorption band centered ~535 nm, which can be ascribed to the bleaching of the ground-state of the dye. Moreover, as shown in the inset of Fig. 7, the absorption kinetic profiles measured at 350, 430 and 760 nm and the recovery of the bleaching (535 nm) followed first-order kinetics with identical lifetimes. From these results, it is possible to conclude that the positive bands observed in the transient spectrum correspond to the MV triplet excited state. Triplet formation was also studied in c-hexane and acetonitrile. Results are

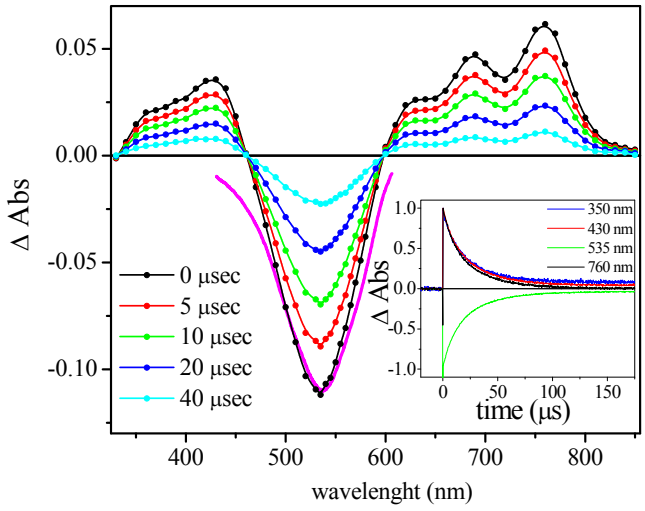

Fig. 7. Time evolution of the transient absorption spectrum of MV in ethyl acetate. Inset: kinetic profiles at 350 nm, 430 nm, 535 nm and 760 nm. Excitation wavelength: 532 nm. The black line corresponds to the transient absorption spectrum extrapolated to $t = 0$. The magenta line shows the (ground state) MV absorption spectrum in the same solvent.

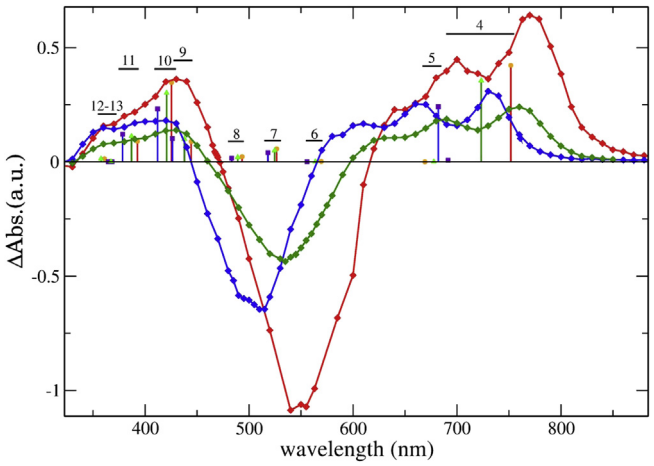

Fig. 8. Transient absorption spectra extrapolated to $t = 0$ for MV in c-hexane (blue), ethyl acetate (green) and acetonitrile (red). Vertical lines represent the MO calculated wavelengths for the $T_1 \rightarrow T_n$ transitions and the corresponding oscillator strengths (f). The values of f are relative numbers represented in an arbitrary scale just for comparison. Actual values are collected in Table 3. (For interpretation of the references to colour in this figure legend, the reader is referred to the web version of this article.)

shown in Fig. 8. As expected, the negative bands shift to higher energies with decreasing solvent polarity following the solvent dependence observed for the ground-state absorption. Interestingly, $T_1 \rightarrow T_n$ transitions follow a similar trend.

A computational characterization of all triplet states up to 400 nm (first 12–13 excited states) was carried out and the energies of $T_1 \rightarrow T_n$ transitions (relative to S_0 in each solvent) compared to that of the transient absorption spectra in Fig. 8 and Table 3. The energies of the states are in good agreement with the experiment and the relative intensities are roughly simulated. The effect of the red shift of all bands with increasing solvent polarity is very well reproduced.

The first three $T_1 \rightarrow T_n$ transitions are not assigned either because they occur in the NIR (outside the experimental window) or have zero intensities. The most intense band corresponds to the $T_1 \rightarrow T_4$ transition in the most polar solvents and to $T_1 \rightarrow T_5$ in c-hexane. In all cases, the final state (T_4 or T_5) is characterized by the same combination of Slater's determinants, with the heavier coefficient for the one corresponding to the HOMO-5 → LUMO excitation. This transition showed a sharp red-shift with increasing solvent polarity (750 cm^{-1} from c-hexane to acetonitrile), fact that can be rationalized in terms of the remarkable increase of the dipole moment of final state compared to that of T_1. The transitions from T_1 to T_6, T_7 and T_8 are hidden by the bleaching of the ground state. The broad band below 450 nm is quite probably composed by three transitions: $T_1 \rightarrow T_9$, $T_1 \rightarrow T_{10}$ and $T_1 \rightarrow T_{11}$. The $T_1 \rightarrow T_{10}$ is the most intense and which shows the larger solvent dependence. This absorption shows a bathochromic shift similar to the lower energy ones ($T_1 \rightarrow T_4 - T_5$). The change in the shape of the spectra is also due to the change in the relative intensity of the $T_1 \rightarrow T_{10}$ band with solvent polarity. Note that although more evident at the longer wavelengths, the red shifts from *c*-hexane to acetonitrile are similar in energy, *i.e.* 750 against 760 cm^{-1}, for the transitions to T_4/T_5 and to T_{10}, respectively. These shifts are also explained by the increase of the dipole moment of the excited triplet state. The electrostatic potential which determines the dipole and spin density distribution which characterizes each electronic state is showed in Fig. 9 for T_1, T_5 and T_{10} triplet states in *c*-hexane.

In order to estimate the triplet quantum yields (Φ_T) in these same solvents, the relative actinometry method [43] was employed. According to this method, the product $\Phi_T\varepsilon_T$ (where ε_T represents the molar absorption coefficient of the triplet state at the wavelength of analysis) can be calculated by comparing the transient absorption intensity of the sample with that of an actinometer. In this study, the triplet–triplet absorption of zinc tetraphenyl porphyrin (ZnTPP) in benzene was used as reference. Values of 7.3×10^4 M^{-1} cm^{-1} and 0.83 were taken for ε_T (at 470 nm) and Φ_T for the porphyrin, respectively [44]. In the practice, the product $\Phi_T\varepsilon_T$ for the MV is calculated according to Equation (6):

$$(\Phi_T\varepsilon_T)_{MV} = \frac{S_{MV}}{S_{ZnTPP}}(\Phi_T\varepsilon_T)_{ZnTPP} \quad (6)$$

where S_{MV} represents the initial slope of a plot of the $T_1 \rightarrow T_n$ absorption of dye (measured at its absorption maximum, see Fig. 7) as a function of the laser energy. Similarly, S_{ZnTPP} is the corresponding slope of the plot obtained for ZnTPP at 470 nm. The absorption of the MV and that of the reference were matched at the excitation wavelength (532 nm). In order to determine Φ_T from the product $\Phi_T\varepsilon_T$ the absorption coefficients of the triplet state of the dye (ε_T) in all solvents must be also calculated. These values were obtained by mean of the ground state depletion (GSD) method [45]. Accordingly, the transient negative difference absorbance estimated at the maximum of the ground state absorption (ΔA_G) was compared with that of the absorption at the maximum of the $T_1 \rightarrow T_n$ spectrum, ΔA_T, both quantities extrapolated to $t = 0$. Thus, the ε_T values are calculated according to Equation (7):

$$\varepsilon_T = \frac{\Delta A_T}{\Delta A_G}\varepsilon_G \quad (7)$$

where ε_T and ε_G represent the molar absorption coefficients of the triplet and ground states, respectively, measured at the wavelengths of their respective maximum (see Fig. 7). The values of ε_G measured in the solvent of interest are listed in Table 1. The values of Φ_T and ε_T in the different solvents are collected in Table 4. The Φ_T obtained are affected by an experimental uncertainty of about 10%. Hence, the values Φ_T are quite similar in all the solvents studied.

Table 3
Calculated properties and experimental wavenumbers for the triplets of MV in the different solvent studied.

Solvent	E_T^N	State	ΔE/cm^{-1}	$T_1^* \rightarrow T_n^*$/cm^{-1}	Observed	f	μ/D	$\Delta\mu$/D	θ/deg
c-Hexane	0.006	T_1^*	10,674	–		–	13.6	–	–
		T_2^*	18,045	7371		0.032	17.0	3.4	2.7
		T_3^*	18,116	7442		0.002	7.1	−6.5	9.9
		T_4^*	25,140	14,466		0.008	15.1	1.5	12.5
		T_5^*	25,336	**14,662**	**13,699**	0.242	16.8	3.2	5.4
		T_6^*	28,665	17,991		0.001	15.1	1.5	3.6
		T_7^*	29,971	19,297		0.041	15.5	1.9	1.5
		T_8^*	31,366	20,692		0.016	15.1	1.5	1.8
		T_9^*	34,133	**23,459**	**23,753**	0.103	15.6	2.0	4.4
		T_{10}^*	34,943	**24,269**		0.232	16.9	3.3	2.0
		T_{11}^*	37,101	**26,427**		0.122	16.0	2.4	0.4
		T_{12}^*	37,828	27,154		0.001	16.5	2.9	9.1
Ethyl acetate	0.228	T_1^*	10,566	–		–	16.6	–	–
		T_2^*	17,103	6537		0.064	21.2	4.6	3.8
		T_3^*	19,213	8647		0	7.2	−9.4	13.4
		T_4^*	24,390	**13,824**	**13,106**	0.355	20.2	3.6	6.0
		T_5^*	25,319	**14,753**	**14,430**	0.005	17.8	1.3	12.8
		T_6^*	28,303	17,737		0.001	18.8	2.2	4.0
		T_7^*	29,630	19,064		0.050	17.8	1.2	1.0
		T_8^*	31,010	20,444		0.020	18.8	2.2	2.5
		T_9^*	33,403	**22,837**	**23,148**	0.101	18.6	2.0	4.3
		T_{10}^*	34,336	**23,770**		0.302	19.9	3.3	2.2
		T_{11}^*	36,411	25,845		0.112	19.9	3.3	0.4
		T_{12}^*	37,792	27,226		0.001	19.5	2.9	9.3
Acetonitrile	0.460	T_1^*	10,493	–		–	18.9	–	–
		T_2^*	16,505	6012		0.091	23.2	4.3	2.3
		T_3^*	19,912	9419		0.000	7.2	−11.6	16.2
		T_4^*	23,796	**13,303**	**12,900**	0.422	22.2	3.3	6.3
		T_5^*	25,437	**14,944**	**14,184**	0.003	19.6	0.7	12.8
		T_6^*	28,053	17,560		0.002	20.8	1.9	3.8
		T_7^*	29,482	18,989		0.057	19.7	0.8	1.1
		T_8^*	30,763	20,270		0.023	21.5	2.6	3.0
		T_9^*	32,998	**22,505**	**22,898**	0.089	20.5	1.6	4.1
		T_{10}^*	33,999	**23,506**		0.347	22.0	3.1	2.3
		T_{11}^*	35,960	25,467		0.090	22.4	3.5	0.4
		T_{12}^*	37,823	27,330		0.002	21.7	2.8	9.4

3.3. Solvent effects on the kinetic parameters of deactivation of MV's singlet excited state

Using the experimental values of Φ_F, τ_F and Φ_T (Tables 1 and 4) the kinetic parameters involved in the deactivation of the singlet excited-state of the MV; *i.e.* the fluorescence (k_F), intersystem crossing (k_{ISC}) and internal conversion (k_{IC}) rate constants, were calculated. The corresponding values are collected in Table 4.

Interestingly, k_F increases with solvent polarity while k_{IC} and k_{ISC} sharply decreases. Note that the non-radiative processes are largely favored in c-hexane. Hence, the very low emission efficiencies observed for MV in the alkane solvents ($\Phi_F \sim 0.002$) is not only the consequence of a decreased k_F but also to a large increase of the non-radiative deactivation rate constants (k_{IC} and k_{ISC}).

The solvents effects on both the radiative and non radiative processes can be qualitatively explained taking into account the theoretically calculated molecular properties of S_1^*. The radiative rate constant (k_F) is related to the oscillator strength (f) of the transition according to: $k_F \cong \nu_F^2 f$. As discussed in Section 3.1, both the energy of the emission maximum and f decrease with decreasing solvent polarity. In the alkane solvents, mixing of the HOMO-1/HOMO → LUMO transitions becomes significant, lowering f and necessarily disfavoring the probability of the

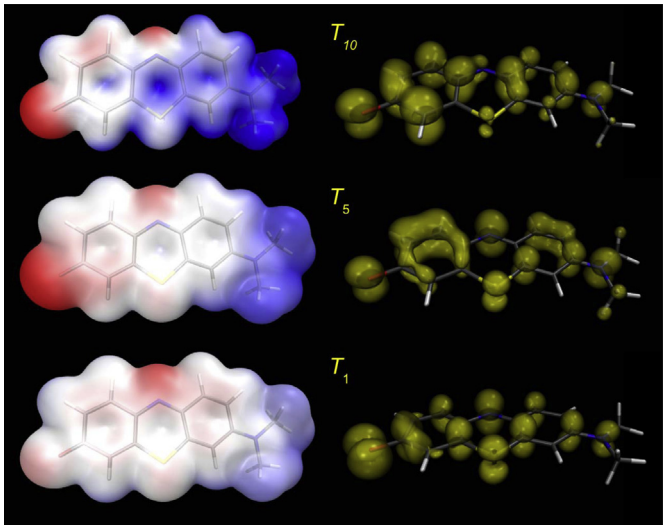

Fig. 9. Electrostatic properties of the triplet states involved in the most intense bands characterized. Left: electrostatic potential, colored on electron isodensity surface of 0.01; color ranges from red (−0.1 a.u.) to blue (+0.1 a.u.). Right: spin density of each triplet plotted at an isodensity value of 0.02*e*. (For interpretation of the references to colour in this figure legend, the reader is referred to the web version of this article.)

Table 4
Molar absorption coefficient of the triplet state (ε_T) at its absorption maximum (ν_T), triplet quantum yield (Φ_T) and kinetic rate constants associated to the deactivation of the singlet excited state of MV in the solvents studied.

Solvent	E_T^N	ν_T/ cm^{-1}	ε_T/ M^{-1} cm^{-1}	Φ_T	k_F/ 10^8 s^{-1}	k_{IC}/ 10^8 s^{-1}	k_{ISC}/ 10^8 s^{-1}
c-hexane	0.006	13,700	14,000	0.55	0.08	17.9	22.5
ethyl acetate	0.228	13,160	17,400	0.48	0.82	3.17	3.70
acetonitrile	0.460	12,990	18,600	0.51	1.21	1.85	3.19

spontaneous emission process. The distorted geometry of S_1^* also explains the large value of k_{IC} in the nonpolar media. Internal conversion is a horizontal transition taking place between S_1^* and S_0 energy surfaces. The magnitude of k_{IC} depends on the Frank-Condon (FC) factor: $\langle \chi_{S_0(\nu=n)} | \chi_{S_1^*(\nu=0)} \rangle$; *i.e.* on the efficiency of overlap between the wavefunction (χ) of the lower vibronic ($\nu = 0$) of the initial state (S_1^*) and the wavefunctions of the vibronic excited states of the final state (S_0). It is well known that the FC factor increases when the nuclear equilibrium coordinates of the involved states differ. As discussed in Section 3.1, the geometry of S_1^* undergoes significant changes in going from polar to nonpolar media, what explains the solvents effects observed on the experimental k_{IC}.

The characterization of the whole set of MV's triplets bellow 400 nm (Table 3) allows the rationalization of the strong dependence of k_{ISC} with solvent polarity. Intersystem crossing (k_{ISC}) can take place either by direct spin-orbit coupling of S_1 to the higher vibrational levels of T_1 or by spin-orbit coupling to one of the higher states T_n, followed by fast internal conversion $T_n \rightarrow T_1$. The rate-determining step is the spin inversion and therefore, the rate constant values of k_{ISC} depend on the extent of spin-orbit coupling as well as, on the energy gap between the states involved (ΔE_{ST}). Selection rules for ISC are given by El Sayed's rule, which predicts that k_{ISC} can relatively large if the $S_1 \rightarrow T_n$ transition involves a change of the molecular orbital symmetry [46]. In order to investigate the viability of all possible $S_1 \rightarrow T_n$ transitions, the energies of the first eight states (singlet or triplets, up to 7500 cm^{-1} above the energy of S_1^*) were recalculated at the nuclear coordinates of the relaxed singlet which is the relevant structure in considering the emission process. The energies of the excited states at the coordinates of S_1^* are plotted as a function of the polarity of the media (E_T^N) in Fig. 6. As shown, $T_1^*(\pi-\pi^*)$ and $T_2^*(\pi-\pi^*)$ lay bellow $S_1^*(\pi-\pi^*)$ in all solvents studied. However, crossing from S_1^* to any of these triplet states is forbidden according El-Sayed's rule. In fact, $T_3^*(n-\pi^*)$ is the only triplet state available with the appropriate symmetry for allowed S/T crossing. The relative energy of this state is quite sensitive to the polarity of the medium. In polar solvents $T_3^*(n-\pi^*)$ is found ~3000 cm^{-1} above S_1^* but its energy progressively decreases until matching that of S_1^* in the alkane solvents. This strongly suggests that the intersystem crossing (ISC) mechanism may vary with the solvent polarity. In the polar solvent series, ISC should involve the forbidden (but energetically favorable) $S_1^*(\pi-\pi^*) \rightarrow T_2^*(\pi-\pi^*)$ transition. The ΔE_{ST} between S_1^* and T_1^* is larger than 7000 cm^{-1} and therefore, this triplet state should not play any significant role in the deactivation process. The value of $k_{ISC} \sim 3.2 \times 10^8\ s^{-1}$ measured for MV in acetonitrile is in good agreement with the rates reported for similar El-Sayed forbidden ISC processes occurring between closely spaced S/T states; for instance anthracene ($k_{ISC} > 10^8\ s^{-1}$) and acetone ($k_{ISC} \sim 5 \times 10^8\ s^{-1}$). In the alkanes solvents (and possibly in *t*-butyl ether), ISC should go *via* the allowed $S_1^*(\pi-\pi^*) \rightarrow T_3^*(n-\pi^*)$ crossing. Note that both conditions for relatively fast ISC process to occur are fulfilled in these media. The large value of k_{ISC} (~$2.2 \times 10^{10}\ s^{-1}$) measured for MV in c-hexane is of the same order of magnitude of the reported k_{ISC} for 9-acetoanthracene (~$10^{10}\ s^{-1}$) and benzophenone (~$10^{10}\ s^{-1}$), which also undergo El-Sayed allowed ISC processes between matching S/T states belonging to different symmetries.

4. Conclusions

Confirming Otsuki et al. [7,8] observations, MV shows a very unusual solvatochromism and a large dependence of the singlet excited decay pathways on the solvent polarity. However, the atypical photophysics of MV is not due to the coexistence of two emitting excited states, as proposed before, but to the combination of a large permanent dipole and a high polarizability of the dye. MV behaves as a typical push–pull chromophore.

It is worth to remark the contribution from the computational simulations for understanding the photophysics of MV. Note that the second singlet (which f is too weak for being observed in the absorption spectra), the change in the electronic topology of the emitting singlet S_1^* (*via* the mixing S_1^*/S_2^* or HOMO-1/HOMO → LUMO) as well as, the study of deaf or hidden triplets, are not accessible by direct experiments. However, the change described for the properties of the relaxed S_1^* plays a role in the peculiar shifts observed in the fluorescence as discussed in the previous section, and it could also be related to the non radiative pathways since both phenomena are clearly different in c-hexane and butyl ether compared to the more polar solvents. In addition, the availability of the closer triplet of the appropriate symmetry for assisting the intersystem crossing in the former is absent in the latter series, it rationalizing again the different trends.

Appendix A. Supplementary data

Supplementary data related to this article can be found at http://dx.doi.org/10.1016/j.dyepig.2014.07.022.

References

[1] Skripchenko A, Robinette D, Wagner SJ. Comparison of methylene blue and methylene violet for photoinactivation of intracellular and extracellular virus in red cell suspensions. Photochem Photobiol 1997;65:451–5.
[2] Wainwright M. Methylene blue derivatives – suitable photoantimicrobials for blood product disinfection? Int J Antimicrob Ag 2000;16:381–94.
[3] Wainwright M, Giddens RM. Phenothiazinium photosensitisers: choices in synthesis and application. Dyes Pigments 2003;57:245–57.
[4] De Nicola R, Walker GM. Accumulation and cellular distribution of zinc by brewing yeast. Enzyme Microb Tech 2009;44:210–6.
[5] Vreeke M, Maidan R, Heller A. Hydrogen peroxide and beta-nicotinamide adenine dinucleotide sensing amperometric electrodes based on electrical connection of horseradish peroxidase redox centers to electrodes through a three-dimensional electron relaying polymer network. Anal Chem 1992;64:3084–90.
[6] Ashassi-Sorkhabi H, Seifzadeh D, Hosseini MG. EN, EIS and polarization studies to evaluate the inhibition effect of 3H-phenothiazin-3-one, 7-dimethylamin on mild steel corrosion in 1 M HCl solution. Corros Sci 2008;50:3363–70.
[7] Otsuki S, Taguchi R. Solvent-dependent photophysical properties of a phenothiazone dye as an optical probe. Bull Chem Soc Jpn 1996;69:2525–31.
[8] Otsuki S, Taguchi R. Solvent-dependent photophysical properties of aminophenoxazone dyes as optical probes. J Photochem Photobiol a: Chem 1997;104:189–95.
[9] Rettig W. Charge separation in excited states of decoupled systems—TICT compounds and implications regarding the development of new laser dyes and the primary process of vision and photosynthesis. Angew Chem Int Ed Engl 1986;25:971–88.
[10] Ronzani F, Trivella A, Arzoumanian E, Blanc S, Sarakha M, Richard C, et al. Comparison of the photophysical properties of three phenothiazine derivatives: transient detection and singlet oxygen production. Photochem Photobiol Sci 2013;12:2160–9.
[11] [See for instance]: a) Thompson WH, Blanchard-Desce M, Hynes JT. Two valence bond state model for molecular nonlinear optical properties. Nonequilibrium solvation formulation. J Phys Chem 1998;102:7712–22;
b) Lu D, Chen G, Perry JW, Goddard III WA. Valence-bond charge-transfer for nonlinear optical properties of charge-tranfer organic molecules. J Am Chem Soc 1994;116:10679–105685 [and references therein].
[12] Painelli A, Terenziani F. A non-perturbative approach to solvatochromic shifts of push–pull chromophores. Chem Phys Lett 1999;312:211–20 [and references therein].
[13] a) Bertolino CA, Ferrari AM, Barolo C, Viscardi G, Caputo G, Coluccia S. Solvent effet on indocyanine dyes: a computational approach. Chem Phys 2006;330:52–9;
b) Kowalczyk M, Sikorska E, Khmelinskii IV, Komasa J, Insinska-Rak M, Sikorski M. Spectroscopy and photophysics of flavin-related compounds: isoalloxazines. J Mol Struct THEOCHEM 2005;756:47–54;
c) Leng W, Wurthener F, Meyer Kelley A. Solvent-depende vrbrational frequencies and reorganization energies of thw merocyanine chromophores. J Phys Chem 2005;109:1570–5.
[14] Mohammad T, Morrison H. Simultaneous determination of methylene violet, halogenated methylene violet and their photoproducts in the presence of

DNA by high-performance liquid chromatography using an internal surface reversed-phase column. J Chromatogr B 1997;704:265–75.
[15] Eaton D. Reference materials for fluorescence measurement. Pure Appl Chem 1988;60:1107–14.
[16] Murov S, Carmichael I, Hug GL. Handbook of photochemistry. 2nd. ed. 1993. New York.
[17] Marcus Y. The properties of organic liquids that are relevant to their use as solvating solvents. Chem Soc Rev 1993;22:409–16.
[18] Michels JJ, Dorsey JG. Retention in reversed-phase liquid chromatography: solvatochromic investigation of homologous alcohol-water binary mobile phases. J Chromatogr 1988;457:85–98.
[19] Adamo C, Barone V. Toward reliable density functional methods without adjustable parameters: the PBE0 model. J Chem Phys 1999;110:6158–69.
[20] Becke AD. Density-functional thermochemistry. III. The role of exact exchange. J Chem Phys 1993;98:5648–52.
[21] Becke AD. A new mixing of Hartree-Fock and local density-functional theories. J Chem Phys 1993;98:1372–7.
[22] Yanai T, Tew DP, Handy NC. A new hybrid exchange–correlation functional using the Coulomb-attenuating method (CAM-B3LYP). Chem Phys Lett 2004;393:51–7.
[23] Frisch MJ, Trucks GW, Schlegel HB, Scuseria GE, Robb MA, Cheeseman JR, et al. Gaussian 09, revision A.01. Wallingford CT: Gaussian, Inc.; 2009.
[24] Cancès E, Mennucci B. Comment on "reaction field treatment of charge penetration". J Chem Phys 2001;114:4744.
[25] Cossi M, Barone V. Time-dependent density functional theory for molecules in liquid solutions. J Chem Phys 2001;115:4708.
[26] Improta R, Barone V, Scalmani G, Frisch MJ. A state-specific polarizable continuum model time dependent density functional theory method for excited state calculations in solution. J Chem Phys 2006;125. 054103:1–9.
[27] Tomasi J, Mennucci B, Cammi R. Quantum mechanical continuum solvation models. Chem Rev 2005;105:2999–3093.
[28] Ramirez CL, Trupp L, Bruttomesso A, Amorebieta VT, Vera DMA, Parise AR. Charge transfer properties of Tröger base derivatives. Phys Chem Chem Phys 2011;13:20076–80.
[29] Heaton-Burgess T, Yang W. Structural manifestation of the delocalization error of density functional approximations: C4N + 2 rings and C20 bowl, cage, and ring isomers. J Chem Phys 2010;132:234113.
[30] Rostov IV, Amos RD, Kobayashi R, Scalmani G, Frisch MJ. Studies of the ground and excited-state surfaces of the retinal chromophore using CAM-B3LYP. J Phys Chem B 2010;114:5547–55.
[31] http://www.cmbi.ru.nl/molden/molden.html.
[32] Humphrey W, Dalke A, Schultten K. J Mol Graph 1996;14:33. See also, http://www.ks.uiuc.edu/Research/vmd/.
[33] Kawski A, Bojarski P, Kuklinski B. Estimation of ground- and excited-state dipole moments of nile red dye from solvatochromic effect on absorption and fluorescence spectra. Chem Phys Lett 2008;463:410–2.
[34] Farley RT, Zheng Q, Gladysz JA, Schanze KS. Photophysics of diplatinum polyynediyl oligomers: chain length dependence of the triplet state in sp carbon chains. Inorg Chem 2008;47:2955–63.
[35] Ravi M, Samanta A, Radhakrishnan TP. Excited state dipole moments from an efficient analysis of solvatochromic stokes shift data. J Phys Chem 1994;98:9133–6.
[36] Reichardt C. Solvatochromic dyes as solvent polarity indicators. Chem Rev 1994;94:2319–58.
[37] Acemoioglu B, Arik M, Efeoglu H, Onganer Y. Solvent effect on the ground and excited state dipole moments of flourescein. J Mol Struct Theochem 2001;548:166–71.
[38] Amos A, Burrows B. Solvent-shift effects on electronic spectra and excited-state dipole moments and polarizabilities. Adv Qunatum Chem 1973;7:289–313.
[39] Lombardi JR. Solvatochromic shifts: a reconsideration. J Phys Chem A 1998;102:2817–23.
[40] Lippert VE. Spektroskopische bistimmung des dipolmomentes aromatischer verbindungen im resten angenegten singulettzustand. Z. Electrochem 1957;61:962–75.
[41] Bakhshiev NG, Knyazhanskii MI, Minkin VI, Osipov OA, Saidov GV. Experimental determination of the dipole moments of organic molecules in excited electronic states. Russ Chem Rev 1969;38:740–54.
[42] Fabian J. TDDFT-calculations of Vis/NIR absorbing compounds. Dye Pigments 2010;84:36–53.
[43] Carmichael I, Hug GL. Triplet–triplet absorption spectra of organic molecules in condensed phases. J Phys Chem Ref Data 1986;15:1–426.
[44] Hurley JK, Sinai N, Linschitz H. Actinometry in monochromatic flash photolysis: the extinction coefficient of triplet benzophenone and quantum yield of triplet zinc tetraphenyl porphyrin. Photochem Photobiol 1983;38:9–14.
[45] Bonneau R, Carmichael I, Hug GL. Molar absorption coefficients of transient species in solution. Pure Appl Chem 1991;63:289–99.
[46] El-Sayed MA. Multiple resonance techniques in the study of the magnetic, radiative and nonradiative properties of the triplet state. Pure Appl Chem 1971;24:475–93 [and references therein].